Liquid metal-based stretchable bioelectronic fiber for electrical stimulation and drug delivery in minimally invasive cardiac therapy

Cite as: APL Bioeng. **9**, 026118 (2025); doi: 10.1063/5.0260773
Submitted: 27 January 2025 · Accepted: 13 April 2025 ·
Published Online: 20 May 2025

View Online Export Citation CrossMark

Chanhui Park,[1,2] Yesol Kim,[1,2] Seonghyeon Nam,[1,2] Hyejeong Kang,[3] Joonho Moon,[3] Ji Hoon Kim,[4] Gi doo Cha,[5] Seung-Pyo Lee,[3,6,a)] Sung-Hyuk Sunwoo,[1,7,a)] and Dae-Hyeong Kim[1,2,a)]

AFFILIATIONS

[1]Center for Nanoparticle Research, Institute for Basic Science (IBS), Seoul 08826, Republic of Korea
[2]School of Chemical and Biological Engineering, Institute of Chemical Processes, Seoul National University, Seoul 08826, Republic of Korea
[3]Division of Cardiology, Department of Internal Medicine, Seoul National University Hospital, Seoul 03080, Republic of Korea
[4]School of Mechanical Engineering, Pusan National University, Busan 46241, Republic of Korea
[5]Department of Systems Biotechnology, Chung-Ang University, Ansung 17546, Republic of Korea
[6]Department of Internal Medicine, Seoul National University College of Medicine, Seoul 03080, Republic of Korea
[7]Department of Chemical Engineering, Kumoh National Institute of Technology, Gumi 39177, Republic of Korea

[a)]**Authors to whom correspondence should be addressed:** sproll1@snu.ac.kr; shsunwoo@kumoh.ac.kr; and dkim98@snu.ac.kr

ABSTRACT

Cardiovascular diseases, such as ventricular arrhythmias and heart failure, require timely and effective treatment to prevent disease progression and improve patient outcomes. Current therapeutics, including electrical shock and emergent cardiovascular medications, have significantly contributed to managing these conditions. However, due to their systemic side effects, there are ongoing demands for highly effective localized therapies. In this regard, a soft implantable device has been considered for cardiac applications, but invasiveness in their implantation procedure and difficulty in compact integration of multiple functions are unmet challenges. To address these issues, we develop a stretchable, multi-functional fiber designed for emergent cardiac intervention, offering electrogram recording, electrical modulation, and drug therapy directly at the epicardial surface. With temperature-dependent phase shifting properties of the liquid metal inside the fiber, the stiffened fiber can be implanted into the thoracic cavity without invasive surgery. Once implanted, the softened fiber provides multimodal therapies (e.g., chemotherapy and electrical therapy) tailored to the patient's condition. By tuning the delivery parameters based on continuous electrogram recording, effective and urgent cardiac interventions for severe arrhythmias are demonstrated in an *in vivo* rat model.

I. INTRODUCTION

Cardiovascular disease, the leading cause of death worldwide, often accompanies severe emergency situations, which highlights the need for effective and urgent interventions to improve patient survival rate.[1,2] Current immediate care strategies, including external high-energy electrical shocks and the administration of pharmaceutical agents, have contributed to saving patients' lives,[3–5] but they often result in systemic side effects[6–8] due to their impact on the entire body. For instance, the electrical shock, used in defibrillation therapy, delivers high-voltage impulses (~360 J) to the chest to reinitialize the cardiac rhythm. This high-intensity stimulation, while effective, can induce complications, such as skin burns, myocardial injury, and pro-arrhythmic consequences. The pharmacotherapy, usually administered orally or by injection, is also prone to systemic side effects, such as electrolyte imbalances, unintended impacts on the nervous system, liver toxicity, and hypotension.

To minimize side effects, implantable bioelectronics have been considered as a promising solution for localized and acute interventions.[9–23] These electronics can offer spatially selective modulation to the target region of the body with immediate therapeutic responses.

Furthermore, it can provide closed-loop personalized electrical modulation for individual symptoms on the basis of continuous monitoring of cardiac electrograms. However, the inherent rigidity and bulky design of conventional bioelectronics often cause unintended tissue damage as well as performance deterioration from mechanical mismatch of the device and the tissue.

Recent advances in soft-material-based implantable bioelectronics have partially addressed these issues.[10,11,17,21,23] Among various soft materials,[24–34] liquid metals and nanocomposites have emerged as promising candidates for soft bioelectronics due to their remarkable mechanical and electrical properties. Liquid metals exhibit exceptionally high conductivity ($\sim 3.4 \times 10^6$ S/m) that remains stable under repetitive mechanical deformations.[30,35–41] They are in a liquefied state at physiological temperatures, so their high softness enables seamless integration into soft curvilinear tissues. Specifically, gallium-based liquid metals are known for their biocompatibility, allowing safe interaction with biological tissues, making them ideal for implantable devices.[36,42] Additionally, nanocomposites, composed of elastic polymer and conductive fillers, provide high conductivity as well as stretchability.[20,32,43–47] They also feature tunable functionalities through the incorporation of various nanoparticles, demonstrating low impedance, excellent mechanical durability, and even additional functionalization such as enhanced biosensing capabilities or improved biocompatibility. Despite these advantages, the complexities of soft-material-based bioelectronics still require more intricate and invasive surgical procedures, limiting their use to a small subset of patients. For broader applications such as emergent cardiac conditions, strategies enabling rapid and straightforward implantation are required.

Moreover, conventional cardiac implants rely solely on electrical therapy. Such devices cannot accommodate simultaneous pharmacological treatments due to challenges in drug refills and the need for additional space for drug reservoirs. However, cardiac drug administration plays a critical role not only in managing arrhythmia but also in non-arrhythmic cardiovascular disorders, supporting heart recovery during or after electrical modulation.[48,49] Thus, multimodal therapeutic approaches integrating electrical and pharmacological therapies within an all-in-one cardiac implantable device is essential for a more comprehensive and effective treatment.

Fiber-configured soft-material-based devices present a promising solution for integrating multiple treatment modalities while offering a desirable structure for minimally invasive implantation.[15,17,50–54] Their thin, elongated structure supports multifunctionality, enabling both precise electrical modulation and drug delivery. Additionally, it facilitates easy connections between the target organ and the external electrical systems, minimizing damage at the insertion site. Although these devices have been widely applied to organs such as the brain or gastrointestinal tract,[15,17,50,52,53] their application to the heart remains limited due to the challenges of accommodating the heart's dynamic movements. To design effective fiber-based cardiac implantable devices, three critical requirements must be addressed: (1) incorporation of multiple functions to manage diverse cardiac symptoms or conditions; (2) stable performance under repetitive mechanical deformation from dynamic movements of the heart; and (3) specific strategies for handling soft devices while ensuring minimally invasive implantation.

Here, we present a stretchable, multimodal fiber that can be administered via minimally invasive implantation onto the epicardium, capable of performing electrogram recording, electrical stimulation, and drug administration. Utilizing liquid metal and functionalized nanocomposite, the device manifests stable performance even under the heart's dynamic and harsh conditions. The phase transition property of liquid metal enables rapid and less-invasive implantation, simplifying the surgical procedure while ensuring precise placement. Upon detecting abnormal signals during electrogram recording, electrical stimulations, drug delivery, or a combination of both can be applied to provide targeted treatment, with therapeutic effects monitored in real time. This closed-loop therapeutic system is successfully demonstrated in an *in vivo* rat model.

II. RESULTS

A. Structural design and functional characteristics

The device mainly features a tri-layer structure comprising a central drug channel, an intermediate layer of liquid metal (eutectic gallium–indium, EGaIn), and an outer nanocomposite layer [Fig. 1(a-i)]. The nanocomposite, made of gold-coated silver nanowires (Ag–Au NWs), functions as a biocompatible and low impedance epicardial electrode, leveraging the inertness and high biocompatibility of gold, without losing intrinsic high conductivity of silver [Fig. 1(a-ii) and supplementary material Fig. 1]. Both the nanocomposite and EGaIn exhibit stretchability and strain-insensitive electrical properties, enabling the fiber to reliably transmit electrical signals even in dynamically deforming environments.

The innovative administration method of the fiber, minimally invasive implantation, could be implemented by exploiting the low melting point of EGaIn ($\sim 15\,^{\circ}$C). When cooled below $0\,^{\circ}$C, the fiber becomes rigid, facilitating easy penetration through the skin without invasive surgical tools. Upon reaching body temperature, the EGaIn transitions to low-modulus state, ensuring soft and conformal contact with the delicate epicardial tissue, while minimizing the risk of damage [Fig. 1(a-iii)]. Meanwhile, the central microfluidic channel, fabricated from Ecoflex silicon with an elastic modulus similar to that of the nanocomposite, maintains structural integrity and stable performance under mechanical deformation, thereby preventing delamination. Additionally, the fiber is encapsulated with Ecoflex elastomer, leaving both ends exposed. This supplementary encapsulation layer serves to prevent unintentional interaction with surrounding tissue at the insertion site during the delivery of biophysiological or electrical signals.

By integrating microfluidic channels with conductive materials, the fiber achieves three key multimodal functions: (1) real-time electrogram recording, (2) electroceutical stimulation for immediate intervention, and (3) microfluidic drug delivery directly to the heart to regulate abnormal heart rates and complement electroceutical therapies [Fig. 1(b)]. Electrical stimulation, which provides an immediate effect on heart rate, is particularly effective in acute conditions such as heart failure, cardiac arrest, or ventricular arrhythmias. However, in several cardiovascular diseases, such as atrioventricular block or sick sinus syndrome, electrical stimulation by itself may be insufficient.[55] Pharmacological treatment becomes especially critical in such scenarios, as it could regulate abnormal heart rates that cannot be fully addressed by electrotherapy. Moreover, combining electrical and pharmacological therapies may improve therapeutic outcomes by alleviating complications such as thrombosis or pain associated with only electroceutical interventions.[56]

Due to its multifunctionality and ease of implantation, the fiber is well-suited for emergency applications. When cardiac emergencies

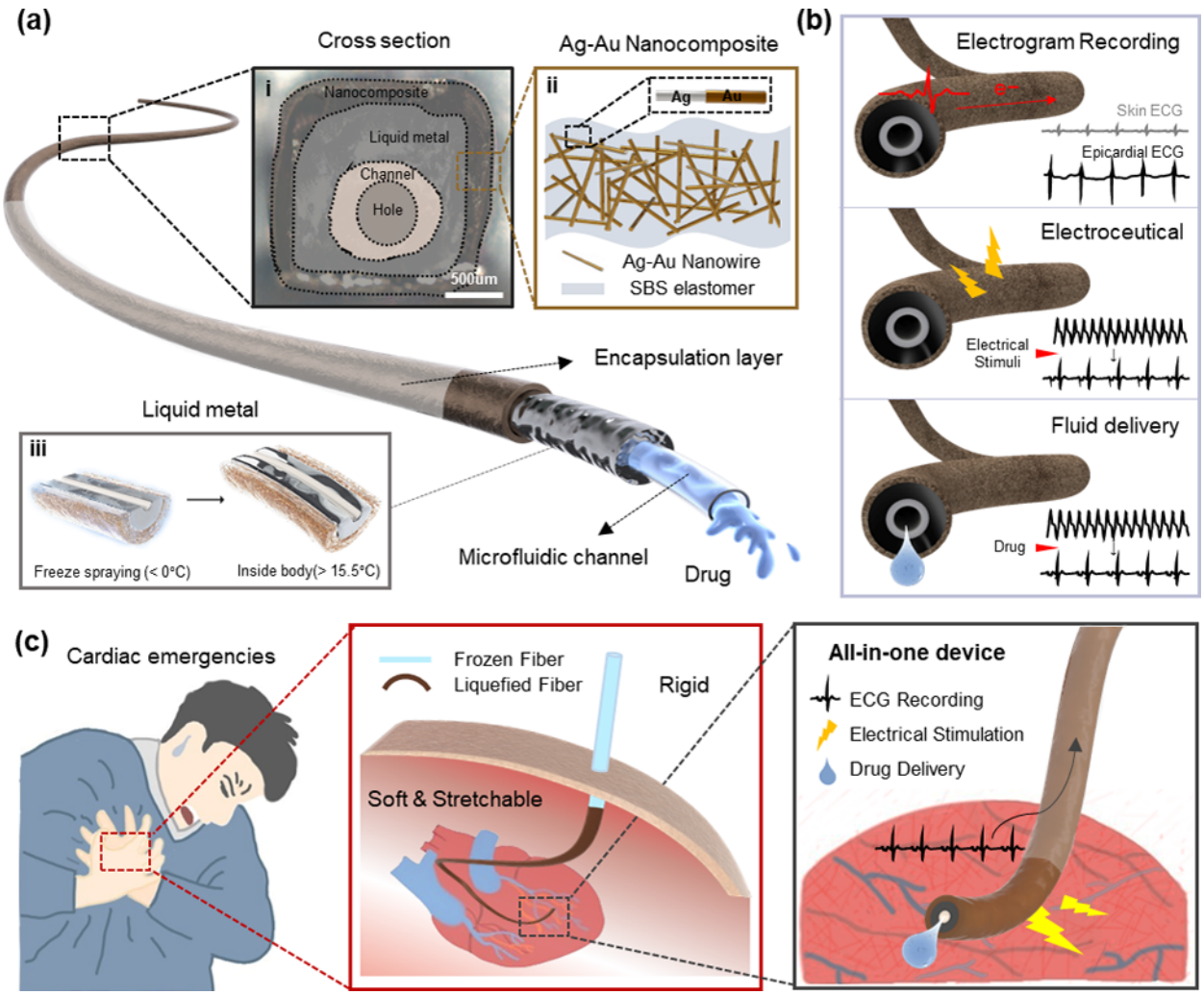

FIG. 1. Device configuration and operating mechanism. (a) The stretchable, cylindrical-shaped fiber, composed of a tri-layer structure, is characterized as follows: (i) a cross-sectional optical microscopic image features inner composition. (ii) The elastomeric outer shell, which consists of a composite of silver–gold core-shell nanowires and SBS polymer, encapsulates (iii) the liquid metal core (eutectic gallium–indium) with a centrally positioned microfluidic channel. The liquid metal transitions between a frozen and liquid state depending on the temperature, enabling minimally invasive implantation. (b) The conductive body and integrated drug channel enable three primary functions, electrogram recording, electrical modulation, and drug delivery. (c) In cardiac emergencies, the frozen fiber rapidly penetrates tissues and transitions to a low-modulus state due to the adaptive modulus properties of the liquid metal. The transition allows the fiber to conform to the epicardial surface. By simultaneously offering multiple operations, the device facilitates effective and immediate therapy.

occur, the fiber can be rapidly implanted using the phase transition properties of the liquid metal. Once implanted, the all-in-one device provides treatment solutions tailored to the condition of patients by monitoring epicardial signals in real time, ensuring an acute and effective closed-loop therapeutic system [Fig. 1(c)].

B. Materials and fabrication process

The elastomeric nanocomposite is prepared through a multi-step process. First, Ag–Au NWs are synthesized by sheathing Ag NWs with gold as previously reported.[46,47] The Ag–Au NWs are then uniformly dispersed in a solution of toluene and ethanol with hexylamine as a dispersant. Separately, styrene–butadiene–styrene (SBS) block copolymer is dissolved in toluene to prepare an elastomer solution. These two solutions are mixed thoroughly via vortexing to form a nanocomposite solution. The mixture is subsequently mold-cast and dried, yielding a nanocomposite with a dense percolation network of Ag–Au NWs embedded within the SBS matrix. This configuration provides the material with excellent electrical conductivity, stretchability, and biocompatibility [Fig. 2(a-i)]. The phase-convertible liquid metal, EGaIn, is encased within the nanocomposite shell [Fig. 2(a-ii)].

The fabrication process of the fiber is illustrated from Figs. 2(b)–2(d). First, the microfluidic channel is prepared by mold-casting Ecoflex. A long metal wire is positioned at the center of a 3D-printed mold, Ecoflex

is poured in and cured, and the wire is subsequently removed to create the hollow microfluidic channel [Fig. 2(b)]. Next, a polydimethylsiloxane (PDMS) mold is prepared to shape the fiber. The PDMS mold design, shown in Fig. 2(c) includes a central section to define the fiber and grooves at both ends for positioning the microfluidic channel centrally within the fiber's cross section.

The final fiber is fabricated by integrating the components described above [Fig. 2(d)]. The nanocomposite solution is blade-coated onto the PDMS mold and dried under ambient conditions, forming a U-shaped nanocomposite film due to capillary forces between the solution and mold surface. EGaIn is then injected into the voids enclosed by the nanocomposite film. The pre-fabricated microfluidic channel is placed along the grooves in the mold, aligning it at the center of the EGaIn layer. A second nanocomposite layer is blade-coated over this structure, encapsulating the EGaIn and microfluidic channel within the nanocomposite shell. After sufficient coating, the

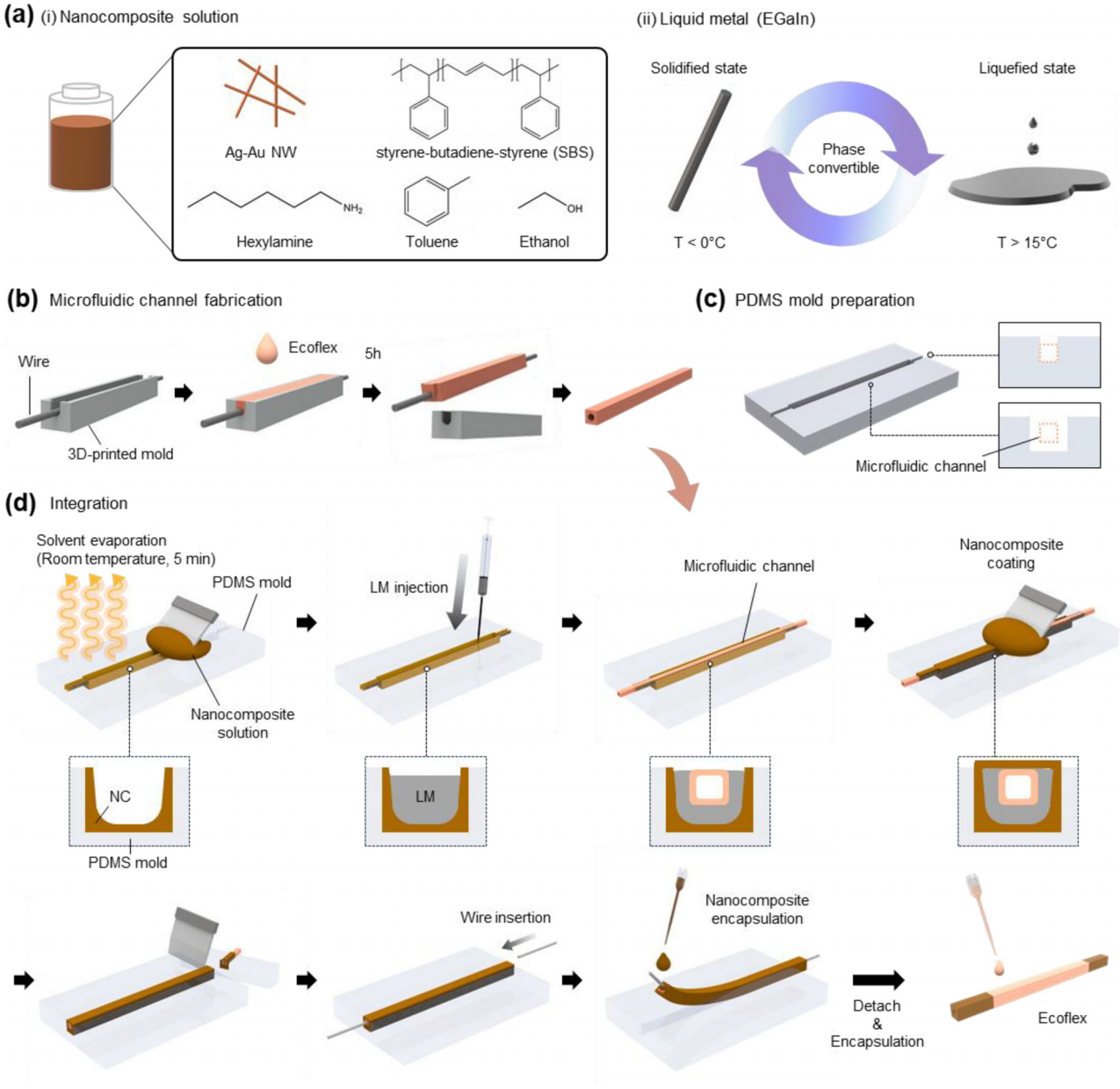

FIG. 2. The schematic illustrating materials and fabrication process. (a) The material requirements for synthesizing the nanocomposite solution and the eutectic gallium–indium alloy as a liquid metal. (b) Fabrication of a microfluidic channel by Ecoflex casting and (c) a customized PDMS mold structure for the outer frame. (d) Step-by-step integration of nanocomposite outer frame, liquid metal, and prepared channel to complete the fabrication of the fiber.

edges of the mold are removed, and both ends of the device are additionally sealed with the nanocomposite material to prevent any leakage of the liquid metal. Finally, to prevent unintentional electrical stimulations in the surrounding tissues, the main shaft is insulated by casting Ecoflex elastomer.

C. Mechanical and electrochemical characterization

Von Mises stress analysis highlights the penetration capabilities of the fiber in its solidified and liquefied states [Fig. 3(a)]. In the solidified state, the fiber exhibits a high elastic modulus (500 MPa) that is superior to the modulus of the breast tissue (3.43 MPa)[57–59] enabling effective penetration on skin for fiber's minimally invasive characteristics. Furthermore, the fiber could maintain structural integrity even under frozen process, as the induced stress remains below the fracture strength (1.66 MPa). Conversely, in the liquid state, the elastic modulus drops to 5 MPa, which implies that the insertion of fiber in liquefied state is impossible. The maximum principal stretch represents the specific ratio of the stretched length to the original length for both solidified and liquefied fiber (supplementary material Fig. 2). These mechanical properties are experimentally validated through tensile tests [Figs. 3(b) and 3(c)], revealing a maximum strain of 250% in the liquid state, indicative of high ductility, and a strain tolerance of up to 50% in the frozen state, reflecting brittle behavior.

The fiber exhibits high stretchability, a critical property for cardiac bioelectronics, with elongation up to 300% without any defects [Fig. 3(d)]. Given the natural stretchability of the heart (∼20%),[24] the stretchability of the fiber is sufficient to withstand the dynamic motion on the heart. In addition, such external deformation rarely affects the electrical property of the fiber. Strain-insensitive electrical properties, essential for maintaining stable performance under extreme conditions, are confirmed in Figs. 3(e)–3(g). The relative resistance change remained below 1 under 80% strain, indicating minimal variation in the resistance under mechanical deformation, making the fiber well-suited for cardiac applications. Additionally, cyclic tests under 30% strain demonstrate consistent electrical performance over repeated loading cycles, validating the durability and reliability of the fiber.

The device's capabilities as bioelectronics are further verified through electrochemical tests [Fig. 3(h)]. Impedance measurements over a 5-h period reveal minimal changes at 1000 Hz, a commonly used frequency for biophysiological recording, demonstrating electrochemical stability [Fig. 3(i)]. Similarly, periodic current density changes in response to cyclic voltage confirm the fiber's durability and repeatability in dynamic environments, underscoring its suitability as a capacitive electrode [Fig. 3(j)]. Cyclic voltammetry analysis reveals a nonlinear current–voltage relationship, showcasing the fiber's combined charge storage and transport properties, further highlighting its functionality as a capacitive electrode [Fig. 3(k)].

D. *Ex vivo* drug delivery demonstration

The fiber delivers drugs to the epicardial surface through its hollow microfluidic channels, with a diameter of 400 μm. Utilizing a straightforward fabrication process, the fiber was designed with multiple drug channels, enabling the simultaneous administration of different drugs (supplementary material Fig. 3). Before use, the fiber should be solidified with a freezing spray to enable skin penetration. After implantation, it re-softens, allowing seamless contact with the epicardial tissue without any damage [Fig. 4(a)]. Since the fiber starts to melt after approximately 40 s of tissue contact, there is sufficient time to reach the epicardium (supplementary material Fig. 4). An *ex vivo* demonstration of the sequential drug delivery process is shown in Fig. 4(b), by using 1 wt% agar hydrogel as an artificial tissue model. The fiber, equipped with a sharp tip and enhanced stiffness due to solidified EGaIn [Fig. 4(c)], could penetrate the artificial tissue to a depth of 3 cm, which is enough to be clinically applicable. Once implanted, it can be softened and slightly bent, while continuing to facilitate the sequential delivery of two mock drugs.

To validate its suitability for *in vivo* application, we evaluated the fiber's drug delivery performance under various conditions [Fig. 4(d)]. The 3D-printed mold allows the fiber to be connected to commercial syringes of various capacities (supplementary material Fig. 5). Among these, a 1 ml syringe was used for flow rate measurements conducted under different conditions. First, the flow rate of the mock drug through the channel was measured under different injection pressures. The flow rate of the fiber was comparable to those of a conventional 31G syringe, ensuring precise dosing control on the epicardium [Fig. 4(e)]. Next, the fiber's performance was tested under bending conditions, maintaining a consistent flow rate even at a bending radius as small as 0.5 cm [Fig. 4(f)]. Additionally, the fiber exhibited reliable drug release performance under repetitive stretching [Fig. 4(g)]. These *ex vivo* experimental findings demonstrate the fiber's suitability for cardiac applications, particularly in dynamic physiological and constrained environments. It ensures precise dosing and maintains durability and functionality during implantation, making it an effective tool for epicardial drug delivery.

E. *In vivo* implantation and electric therapy

To validate the *in vivo* feasibility of the fiber for cardiac monitoring and electrotherapy, we demonstrated its minimally invasive implantation, electrophysiological monitoring, and therapeutic application in a cardiopathologic animal model [Fig. 5(a)]. The sterilized fiber was frozen using a simple ice spray, and the sharpened tip was gently inserted into the thoracic cavity of Sprague–Dawley rats through the intercostal space between the left 3rd and 4th ribs. The implantation process was captured via endoscopic imaging [Figs. 5(b)–5(d)].

The epicardial electrogram (hereafter referred to as "epicardiogram") was recorded and compared to the surface electrocardiogram (ECG) on the same scale to assess recording quality [Fig. 5(e)]. Unlike the conventional surface ECG (black), the epicardiogram (blue) provided clearer signals with higher amplitude (30 mV compared to 0.7 mV) and a superior signal-to-noise ratio (SNR 122 dB compared to SNR 14 dB). This suggests that the epicardiogram can offer spatiotemporally precise information on local cardiac conduction that is unattainable with conventional surface ECGs. Further implementation of an epicardiogram recording in an *in vivo* rabbit model validates the fiber's capabilities as an electrode even in larger animals (supplementary material Fig. 6). Additionally, cardiopathologic conditions, such as ventricular arrhythmias, were detectable through the epicardiogram. For example, ventricular bradycardia was induced by intraperitoneally injecting diltiazem (100 mcg per kg). Before injection, the epicardiogram displayed a normal sinus rhythm with an R–R interval of 179.8 ± 8.4 ms. After injection, the R–R interval increased significantly to 948 ± 14.7 ms, indicating severe bradycardia [Fig. 5(f)]. To demonstrate therapeutic efficacy, electrical stimulation (1.2 V amplitude, 5 ms pulse duration, 360 beats per minute) was applied through the fiber

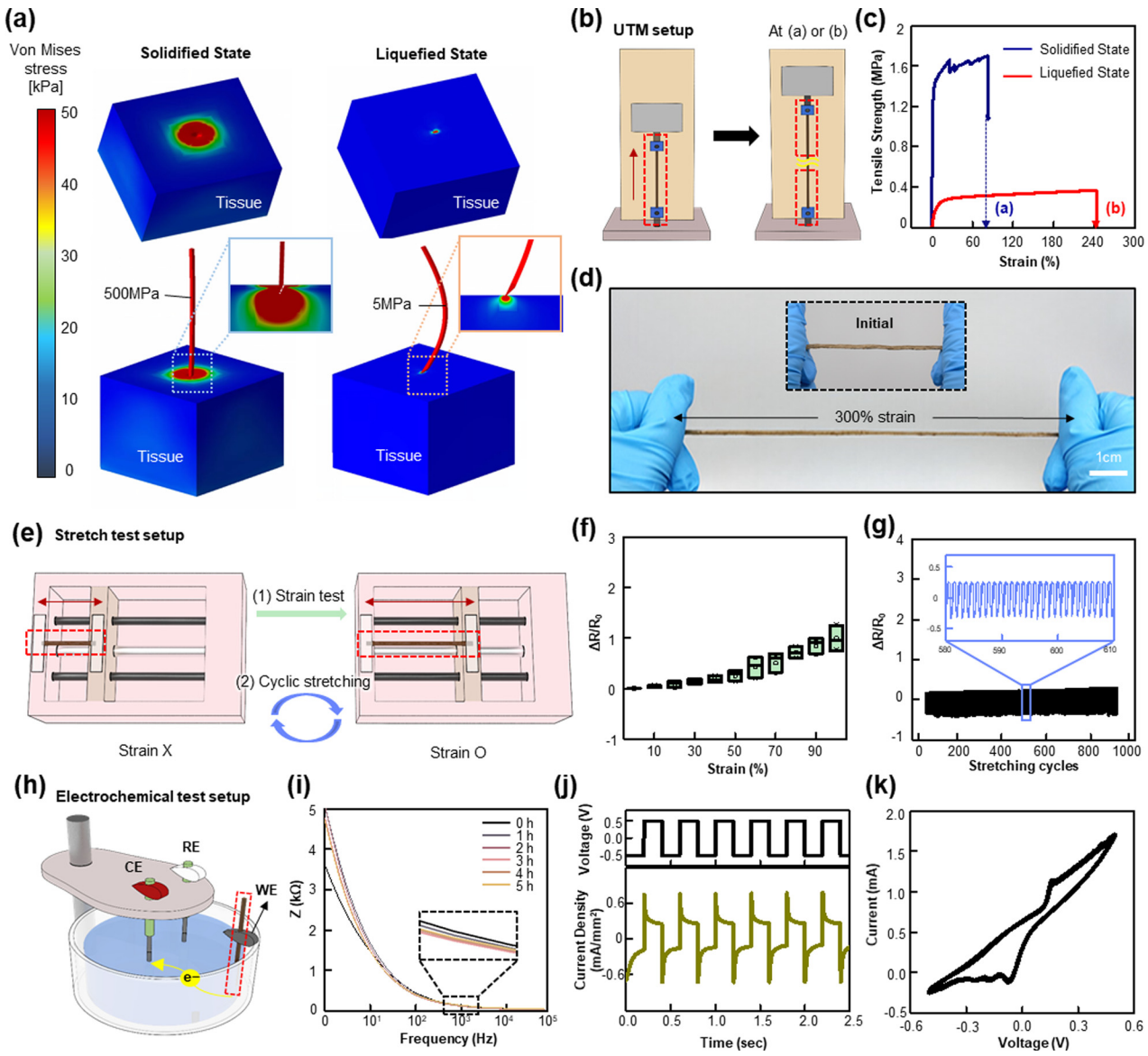

FIG. 3. Mechanical, electrical, and electrochemical characteristics as stretchable bioelectronics. (a) Von mises stress distribution illustrates the response of the fiber in solidified state and normal state during skin penetration. (b) and (c) The stress–strain curve demonstrates the fiber's behavior under load in both states, highlighting key mechanical properties such as elastic modulus and fracture strength. (d) Optical images of the fiber before (inset) and after stretching. (e)–(g) Relative resistance changes (R/R0) during strain testing and cyclic stretching reveal the strain-insensitive electrical properties of the fiber. (h) Electrochemical tests verify the stability and functional capabilities of the fiber as a bioelectronics device. (i) The marginal difference in impedance around 1000 Hz, even after 5 h of exposure to PBS, indicates impedance stability. (j) The current density of the conductive nanocomposite electrode, induced by voltage pulses, demonstrates charge injection capacity, while (k) cyclic voltammetry present charge storage capacity, further showcasing the potential as an electrode.

(red upward triangles). The ventricular contractions were successfully synchronized with the electrical pacing, restoring the R–R interval to 166.6 ms, within the normal range for rats.

The fiber also effectively addressed ventricular tachycardia, a potentially fatal arrhythmia [Fig. 5(g)]. Tachycardia was induced by injecting norepinephrine (10 mcg per kg) following left anterior descending coronary artery ligation. The fiber accurately recorded the disorganized, rapid contractions associated with tachycardia. Since the arrhythmia did not resolve spontaneously, overdrive pacing (2 V amplitude, 1 ms pulse duration, and 10 Hz frequency) was delivered via the fiber for 10-s intervals until cardiac resynchronization was achieved.

F. Drug delivery and synergistic therapies

To extend its functionality beyond isolated electrotherapy, the fiber's drug delivery capabilities were evaluated. Its dual-channel

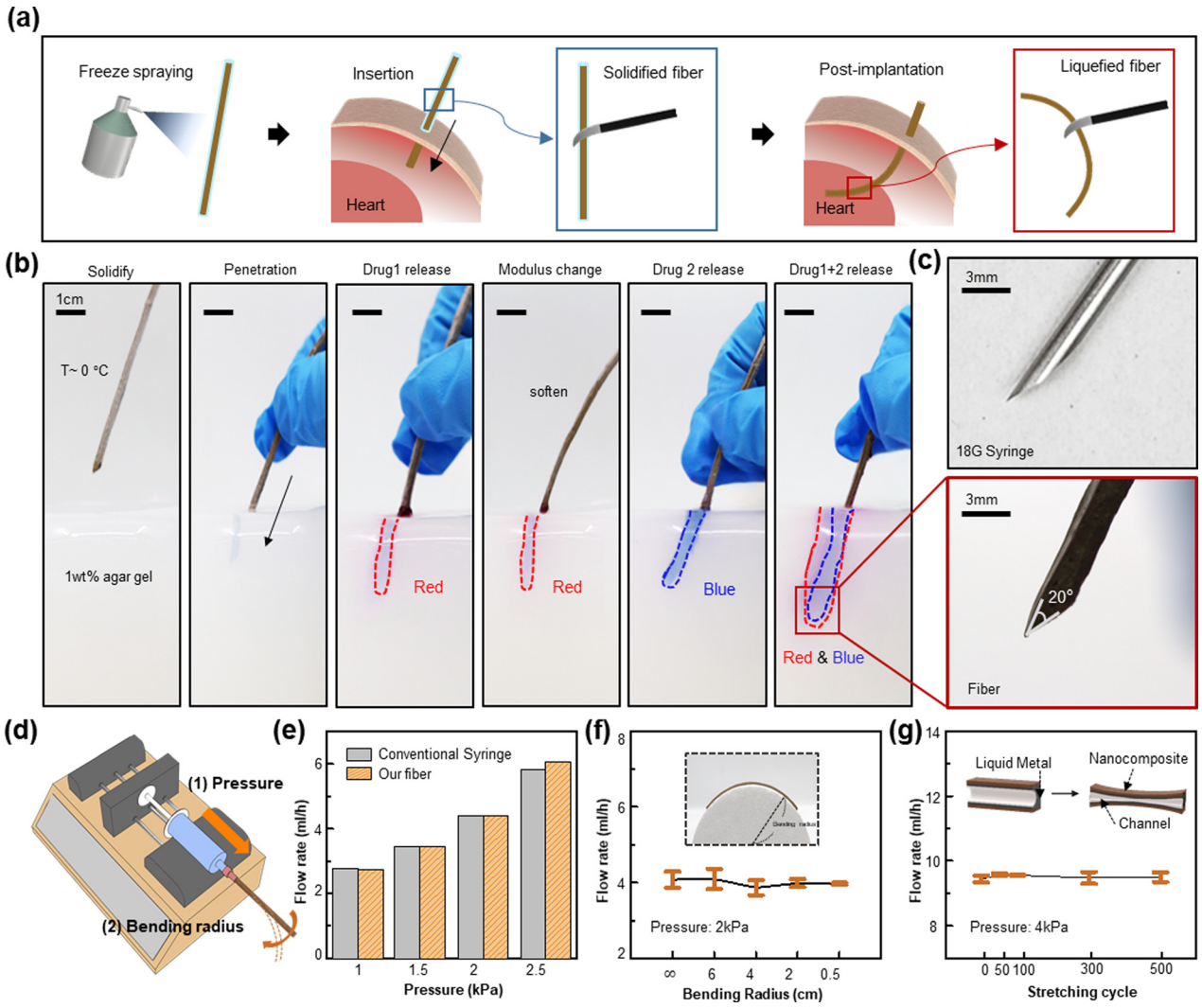

FIG. 4. Fluidic delivery *ex vivo* demonstration and performance evaluation. (a) The process of minimally invasive implantation using freeze spraying. (b) The multiple drug delivery is validated in an *ex vivo* experiment using 1 wt% agarose gel. (c) The end of the fiber is sharpened like conventional needle, allowing for easy penetration. (d) A syringe pump is used to maintain constant pressure, and (e) the fiber achieves a flow rate similar to a conventional syringe, depending on the applied pressure. (f) The fiber maintains a consistent flow rate under various bending radius and (g) across different stretching cycles.

microfluidic system allowed for sequential drug delivery onto the epicardial surface. As a demonstration of its multi-drug delivery capability, mock drugs (red and blue dyes) were injected sequentially and simultaneously [Figs. 6(a)–6(d)]. The first mock drug (red dye) was successfully delivered [Fig. 6(b)], followed by the second (blue dye) through a separate channel [Fig. 6(c)]. Simultaneous injection of both dyes produced a violet-like color [Fig. 6(d)], demonstrating the potential for hybrid drug delivery.

To test pharmaceutical applications, drugs with physiological effects were delivered to the epicardial surface. The fiber was implanted, ensuring the drug channels were in contact with the epicardial surface. At rest, the initial R–R interval was 281.96 ± 2.03 ms. Epinephrine (1 mcg per kg) was injected, increasing heart rate and cardiac pressure, reducing the R–R interval to 203.04 ± 0.18 ms. Subsequently, diltiazem (10 mcg per kg) was administered through the second channel, slowing the heartbeat and increasing the R–R interval to 417.32 ± 1.23 ms. To demonstrate the synergistic effect of electrotherapy and chemotherapy, electrical stimulation was applied to restore the heartbeat to normal ranges, reducing the R–R interval to 166.7 ms. All R–R interval changes were statistically significant ($p < 0.005$) [Figs. 6(e) and 6(f)].

To evaluate the physiological feasibility of epicardial drug delivery, diltiazem was administered to seven groups of mice ($n = 5$ per group) via different methods: subcutaneous (s.q.), intramuscular (i.m.), intraperitoneal (i.p.), intravenous (i.v.), and epicardial injection (a dose of 10 mcg/kg was administrated for s.q., i.m., i.p., and i.v., and three levels of dose—10, 5, and 1 mcg/kg—were used for epicardial injection) [Figs. 6(g)–6(i)]. Among conventional methods, intravenous

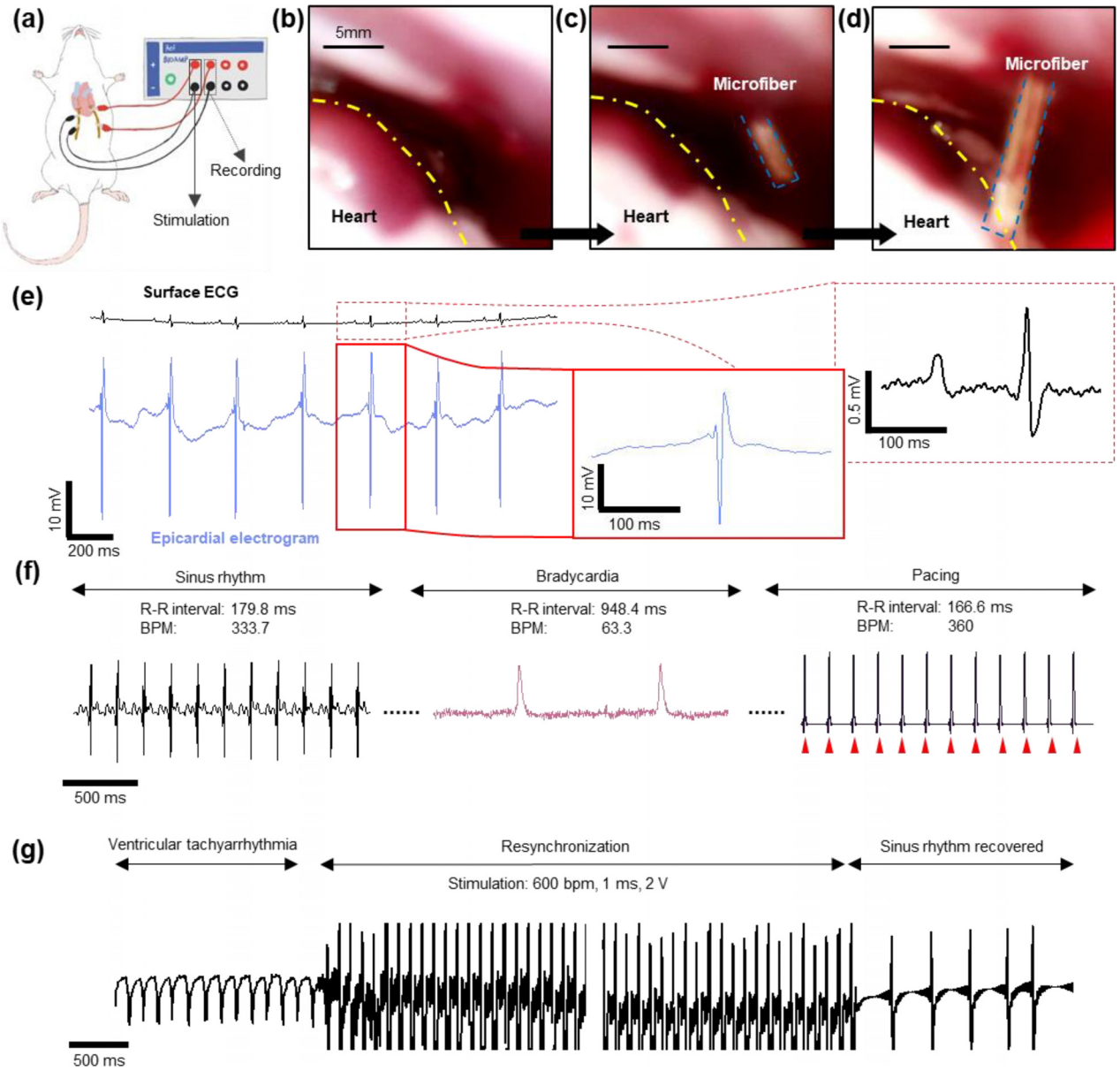

FIG. 5. Cardiac application of the fiber in terms of recording and electroceutical functionality. (a) Schematic illustration demonstrating the setup of an *in vivo* rat model experiment, highlighting simultaneous electrogram recording and electrical stimulation. Optical endoscope image captured during minimally invasive fiber implantation: (b) before implantation, (c) during implantation, and (d) showing secure contact with the heart. (e) Comparison of the recorded epicardial electrogram's intensity with skin ECG. (f) Epicardial electrograms of normal heart, bradycardia, and during pacing. (g) Epicardial electrogram during ventricular tachycardia, resynchronization therapy, and post recovery.

injection exhibited the fastest effect. Interestingly, epicardial injection provided an even faster response than i.v. administration, even at lower doses (10%). These results highlight the fiber's potential for precise, localized drug delivery with reduced dosage requirements, making it a promising tool for addressing cardiac emergencies.

For clinical translation, however, additional advancement is required. In this study, as clinicians evaluated the disease based on recorded electrogram and implemented treatments, the time delay was inevitable, limiting the device's potential application in emergent situations. By incorporating automatic disease classification and treatment using an add-on device, significantly faster and more precise interventions could be achieved. To demonstrate this potential, we developed a cardiac disease classification code using MATLAB with the epicardial electrogram signals collected from the fiber, as shown in Fig. 6(j) and supplementary material Fig. 7. This MATLAB code processes the signal to enhance the QRS complex and detects actual R-peak positions

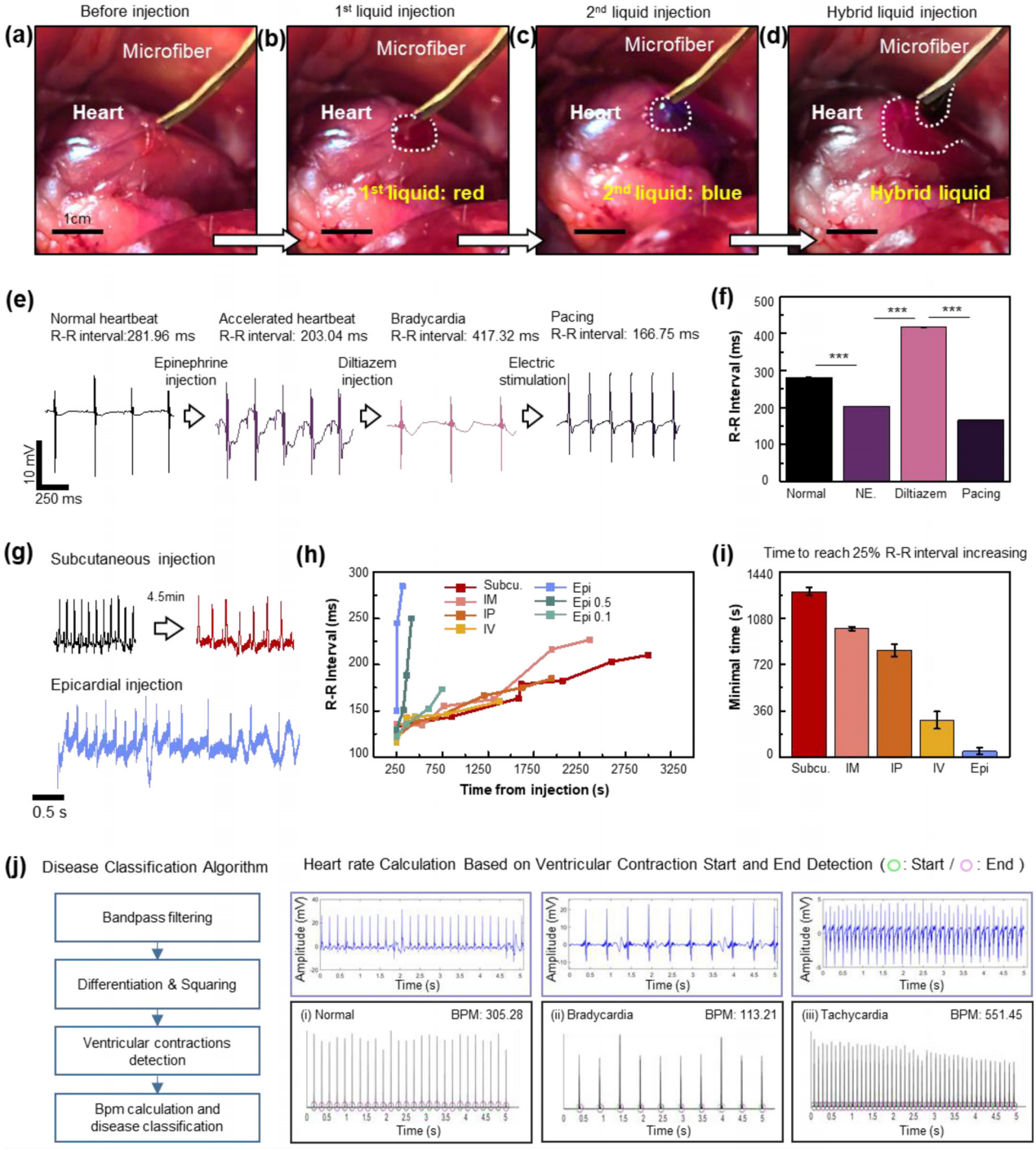

FIG. 6. *In vivo* demonstration of drug delivery and performance evaluation. (a) Optical image of the drug administration process: before injection, (b) during first type of drug injection, (c) the second type of drug injection, and (d) the combined type of drug injection. (e) Transitions of the epicardial electrogram observed during sequential delivery of epinephrine, diltiazem and electrical signals. (f) Comparison of the R–R interval between normal and after administration of epinephrine, diltiazem, and electrical stimulation. (g) Instantaneous heart rate changes compared to subcutaneous injection. (h) Transition of the R–R interval over time following injection, based on the injection method. (i) Comparison of response times based on the injection method. The response time is defined as the point when the R–R interval increases to 125% of its baseline value. (j) Disease classification code (MATLAB) and the result when applied to normal, bradycardia, and tachycardia electrogram. By detecting the number of ventricular contractions, the code can accurately classify the manifestation of the arrythmia.

within segments that exceed a predefined threshold. The heart rate is then calculated based on the number of detected R-peaks and the total duration of the recording. By comparing the calculated heart rate with known reference values for normal rat heart rates, cardiac disease classification can be effectively performed.

III. CONCLUSION

In this study, we developed a stretchable fiber optimized for cardiac emergency applications, integrating multimodal functionality with a design tailored for rapid and straightforward implantation. Constructed from a nanocomposite and EGaIn, the fiber demonstrates exceptional stretchability and strain-insensitive electrical properties, enabling continuous electrogram recording and reliable electrical signal delivery, even under dynamic motion of the heart. The fiber's adaptive modulus, achieved through the temperature-responsive phase transition behavior of EGaIn, facilitates minimally invasive and instantaneous implantation. Furthermore, the incorporation of a microfluidic channel into the fiber allows for stable and durable delivery of multi-drugs, enhancing potential treatment efficacy. Throughout the *in vivo* experiment, the fiber enabled continuous epicardiogram monitoring and targeted treatments based on arrhythmia manifestations, effectively demonstrating the efficacy of a close-loop therapeutic system. Notably, the faster response time of direct epicardial drug administration compared to conventional injection methods highlights the potential as a rapid and efficient intervention for cardiac emergencies.

IV. METHODS

A. Materials

Solvents such as ethylene glycol, ethyl alcohol, acetone, and toluene were purchased from Samchun Chemicals (Republic of Korea). Poly(styrene-butylene-styrene) (SBS, KTR 103) was acquired from Kumho Chemicals (Korea). Liquid metal (eutectic gallium–indium) and hexylamine were purchased from Sigma Aldrich (USA). Ecoflex elastomer was obtained from Hyup-shin corporation. Gold-coated silver nanowires were synthesized as previously reported.[43,47] The connector between the conventional syringe and the fiber was polyJet 3D-printed using VeroWhite photopolymer resin.

B. Preparation of the Ag–Au nanocomposite

The nanocomposite was prepared by mixing Ag–Au nanowires with SBS polymer. The SBS polymer was dissolved in toluene solvent at a weight ratio of 1:10 to form a polymer solution. Simultaneously, a solution of Ag–Au nanowires was prepared at a concentration of 50 mg/ml in a mixed solvent of ethanol and toluene at a ratio of 1:3. The two solutions were combined and thoroughly mixed using vortexing, followed by the addition of hexylamine (20 μl) as a dispersant.

C. Ansys finite element analysis simulation

The tissue was modeled as a cubic box with a side length of 70 mm. The base of the cube was determined as a fixed surface, meaning it could not undergo deformation. All other surfaces, except for the fixed surface, were allowed to deform under loading. The fiber was modeled as a rectangular box with dimensions of 2 mm in the x-direction, 2 mm in the y-direction, and 100 mm in the z-direction and the tip was beveled at an angle of 20°. The base of the fiber was in contact with the top surface of the tissue, with their centers aligned at the same point. Young's modulus was set to 25 kPa for the tissue, 5 MPa for the fiber in the liquefied state, and 500 MPa for the fiber in the frozen state, as determined from UTM measurement. Poisson's ratios of 0.5 for the tissue and 0.43 for the fiber, in both solidified and liquefied states, were applied. A force was loaded on a free xy-surface of the fiber in the z-direction until the surface moved by 5 mm in the z-direction.

D. Mechanical and electrical characterization

A tensile test was conducted to evaluate the stretchability and compare the elastic modulus of the fibers in dual state; solidified and liquefied. The test was performed using a UTM with the stretching speed of 50 mm/min, following a modified ISO 527. The resistance of the fiber under strain and during cyclic experiments was measured using a four-point probe connected to a source meter (Keithley 2450). For sample preparation, the fiber was transferred onto the VHB tape, and Cu wires were attached to the fiber's surface using silver paste for electrical connection. In the strain test, the fiber was initially 1 cm long and stretched by 1 mm increments up to 100% strain for ten cycles. In the cyclic test, the fiber with an initial length of 1 cm, was subjected to 30% strain for 1000 cycles at a frequency of 0.1 Hz.

E. Electrochemical characterization

Electrochemical properties of the fiber as a bioelectronic were evaluated using an electrochemical workstation (CHI-660E, CH instruments). The fiber was immersed in a PBS solution with an exposed area of 45 mm^2. Two Pt electrodes were used as reference and counter electrodes, respectively. Impedance measurements were performed over a frequency range of 1–0.1 MHz with an amplitude of 5 mV. The charge injection capacity was determined by applying an AC pulse with an amplitude of 0.5 V, a pulse width of 0.2 s, and a sensitivity of 0.01 A/V. Cyclic voltammetry curves were obtained from −0.5 to 0.5 V at a scan rate of 100 mV/s.

F. *In vivo* cardiac implantation

All animal experiments were performed under approval of Seoul National University IACUC (SNU-221102-3). The 8-week-old male SD rats (Orient Bio Inc., Korea) were anesthetized with 3%–5% isoflurane chamber. Hair removal using clipper was followed by administration of the commercialized hair removal cream on the left thoracic region. The skin of the intercostal region between the 3rd and 4th rib was poked with an 18G needle. After two microfibers were implanted on the desired location of the epicardial surface, other ends of the microfibers were connected to the commercialized DAQ device, Power Lab (AD Instruments, New Zealand). Norepinephrine was injected intravenously to induce tachyarrhythmias. Otherwise, the diltiazem solution was injected intravenously to induce bradyarrhythmia. To deliver electric stimulation, the pair of microfibers was connected to the current output channel of the DAQ device, Power Lab (AD Instruments, New Zealand). The surface ECG was recorded during stimulation.

G. Statistical analysis

All data are analyzed by the two-sample t test. All statistical indication in the graph presents as mean with standard deviation. Sample size (n) = 5 for experimental data, unless otherwise noted in figure

caption. Statistical details such as p value are described in each figure caption.

SUPPLEMENTARY MATERIAL

See the supplementary material for additional information.

ACKNOWLEDGMENTS

This work was supported by the Institute for Basic Science (No. IBS-R006-A1); the Nano & Material Technology Development Program through the National Research Foundation of Korea (NRF), funded by the Ministry of Science and ICT (No. RS-2024-00450561); and the NAVER Digital Bio Innovation Research Fund, funded by NAVER Corporation (Grant No. 37-2023-0040).

AUTHOR DECLARATIONS

Conflict of Interest

The authors have no conflicts to disclose.

Ethics Approval

Ethics approval for experiments reported in the submitted manuscript on animal or human subjects was granted. All animal experiments were performed under approval of Seoul National University IACUC (SNU-221102-3).

Author Contributions

Chanhui Park, Yesol Kim, and Seonghyeon Nam contributed equally to this work.

Chanhui Park: Conceptualization (equal); Data curation (equal); Formal analysis (equal); Investigation (equal); Methodology (equal); Validation (equal); Visualization (equal); Writing – original draft (equal); Writing – review & editing (equal). **Yesol Kim:** Conceptualization (equal); Data curation (equal); Formal analysis (equal); Investigation (lead); Visualization (equal); Writing – original draft (equal); Writing – review & editing (equal). **Seonghyeon Nam:** Conceptualization (equal); Data curation (equal); Investigation (supporting); Methodology (equal); Visualization (equal); Writing – original draft (equal); Writing – review & editing (equal). **Hyejeong Kang:** Validation (supporting). **Joonho Moon:** Validation (supporting); Writing – review & editing (equal). **Ji Hoon Kim:** Validation (equal); Visualization (supporting). **Gi doo Cha:** Validation (supporting); Writing – review & editing (equal). **Seung-Pyo Lee:** Funding acquisition (lead); Methodology (equal); Project administration (equal); Writing – review & editing (supporting). **Sung-Hyuk Sunwoo:** Conceptualization (equal); Data curation (equal); Formal analysis (equal); Investigation (equal); Methodology (equal); Project administration (equal); Supervision (equal); Validation (equal); Visualization (equal); Writing – original draft (equal); Writing – review & editing (equal). **Dae-Hyeong Kim:** Funding acquisition (equal); Project administration (equal); Supervision (equal); Writing – review & editing (equal).

DATA AVAILABILITY

The data that support the findings of this study are available from the corresponding authors upon reasonable request.

REFERENCES

[1]C. M. Hansen, K. Kragholm, D. A. Pearson, C. Tyson, L. Monk, B. Myers, D. Nelson, M. E. Dupre, E. L. Fosbøl, J. G. Jollis, B. Strauss, M. L. Anderson, B. McNally, and C. B. Granger, "Association of bystander and first-responder intervention with survival after out-of-hospital cardiac arrest in North Carolina, 2010–2013," JAMA **314**(3), 255–264 (2015).

[2]E. J. Benjamin, M. J. Blaha, S. E. Chiuve, M. Cushman, S. R. Das, R. Deo, S. D. De Ferranti, J. Floyd, M. Fornage, C. Gillespie, C. R. Isasi, M. C. Jim'nez, L. C. Jordan, S. E. Judd, D. Lackland, J. H. Lichtman, L. Lisabeth, S. Liu, C. T. Longenecker, R. H. MacKey, K. Matsushita, D. Mozaffarian, M. E. Mussolino, K. Nasir, R. W. Neumar, L. Palaniappan, D. K. Pandey, R. R. Thiagarajan, M. J. Reeves, M. Ritchey, C. J. Rodriguez, G. A. Roth, W. D. Rosamond, C. Sasson, A. Towfghi, C. W. Tsao, M. B. Turner, S. S. Virani, J. H. Voeks, J. Z. Willey, J. T. Wilkins, J. H. Y. Wu, H. M. Alger, S. S. Wong, and P. Muntner, "Heart Disease and Stroke Statistics'2017 update: A report from the American Heart Association," Circulation **135**(10), e146–e603 (2017).

[3]J. Finn, I. Jacobs, T. A. Williams, S. Gates, and G. D. Perkins, "Adrenaline and vasopressin for cardiac arrest," Emergencias **32**(2), 133–134 (2020).

[4]J. P. Marenco, P. J. Wang, M. S. Link, M. K. Homoud, N. A. Mark, and E. Iii, "Improving survival from sudden cardiac arrest the role of the automated external defibrillator," JAMA **285**(9), 1193–1200 (2001).

[5]P. Rossignol, A. F. Hernandez, S. D. Solomon, and F. Zannad, "Heart failure drug treatment," Lancet **393**(10175), 1034–1044 (2019).

[6]D. Hamilton, S. Nandkeolyar, H. Lan, P. Desai, J. Evans, C. Hauschild, D. Choksi, I. Abudayyeh, T. Contractor, and A. Hilliard, "Amiodarone: A comprehensive guide for clinicians," Am. J. Cardiovasc. Drugs **20**(6), 549–558 (2020).

[7]J. Patocka, E. Nepovimova, W. Wu, and K. Kuca, "Digoxin: Pharmacology and toxicology—A review," Environ. Toxicol. Pharmacol. **79**, 103400 (2020).

[8]V. Waldmann, K. Narayanan, N. Combes, D. Jost, X. Jouven, and E. Marijon, "Electrical cardiac injuries: Current concepts and management," Eur. Heart J. **39**(16), 1459–1465 (2018).

[9]Y. J. Hong, H. Jeong, K. W. Cho, N. Lu, and D. H. Kim, "Wearable and implantable devices for cardiovascular healthcare: From monitoring to therapy based on flexible and stretchable electronics," Adv. Funct. Mater. **29**(19), 1808247 (2019).

[10]J. H. Koo, J. K. Song, D. H. Kim, and D. Son, "Soft implantable bioelectronics," ACS Mater. Lett. **3**(11), 1528–1540 (2021).

[11]S.-H. Sunwoo, M.-J. Cha, S. I. Han, H. Kang, Y. S. Cho, D.-H. Yeom, C. S. Park, N. K. Park, S. W. Choi, S. J. Kim, G. Doo Cha, D. Jung, S. Choi, S. Oh, G.-B. Nam, T. Hyeon, D.-H. Kim, and S.-P. Lee, "Ventricular tachyarrhythmia treatment and prevention by subthreshold stimulation with stretchable epicardial multichannel electrode array," Sci. Adv. **9**(13), eadf6856 (2023).

[12]A. A. Hussein and B. L. Wilkoff, "Cardiac implantable electronic device therapy in heart failure," Circ. Res **124**(11), 1584–1597 (2019).

[13]W. Whyte, E. T. Roche, C. E. Varela, K. Mendez, S. Islam, H. O'Neill, F. Weafer, R. N. Shirazi, J. C. Weaver, N. V. Vasilyev, P. E. McHugh, B. Murphy, G. P. Duffy, C. J. Walsh, and D. J. Mooney, "Sustained release of targeted cardiac therapy with a replenishable implanted epicardial reservoir," Nat. Biomed. Eng. **2**(6), 416–428 (2018).

[14]P. Gutruf, R. T. Yin, K. B. Lee, J. Ausra, J. A. Brennan, Y. Qiao, Z. Xie, R. Peralta, O. Talarico, A. Murillo, S. W. Chen, J. P. Leshock, C. R. Haney, E. A. Waters, C. Zhang, H. Luan, Y. Huang, G. Trachiotis, I. R. Efimov, and J. A. Rogers, "Wireless, battery-free, fully implantable multimodal and multisite pacemakers for applications in small animal models," Nat. Commun. **10**(1), 5742 (2019).

[15]T. D. Yoshida Kozai, N. B. Langhals, P. R. Patel, X. Deng, H. Zhang, K. L. Smith, J. Lahann, N. A. Kotov, and D. R. Kipke, "Ultrasmall implantable composite microelectrodes with bioactive surfaces for chronic neural interfaces," Nat. Mater. **11**(12), 1065–1073 (2012).

[16]L. W. Kleiner, J. C. Wright, and Y. Wang, "Evolution of implantable and insertable drug delivery systems," J. Controlled Release **181**(1), 1–10 (2014).

[17]S. Park, H. Yuk, R. Zhao, Y. S. Yim, E. W. Woldeghebriel, J. Kang, A. Canales, Y. Fink, G. B. Choi, X. Zhao, and P. Anikeeva, "Adaptive and multifunctional hydrogel hybrid probes for long-term sensing and modulation of neural activity," Nat. Commun. **12**(1), 3455 (2021).

[18]J. Ausra, M. Madrid, R. T. Yin, J. Hanna, S. Arnott, J. A. Brennan, R. Peralta, D. Clausen, J. A. Bakall, I. R. Efimov, and P. Gutruf, "Wireless, fully implantable cardiac stimulation and recording with on-device computation for closed-loop pacing and defibrillation," Sci. Adv. **8**, eabq7469 (2022).
[19]Z. Shi, X. Gao, X. Cai, H. Zhao, X. Wang, L. Zhao, L. Yin, H. Ding, and X. Sheng, "Fully implantable and retrievable upconversion waveguides for photodynamic therapy in deep tissue," Adv. Opt. Mater. **11**(19), 2300689 (2023).
[20]H. J. Kim, H. Choi, D. H. Kim, and D. Son, "Stretchable functional nanocomposites for soft implantable bioelectronics," Nano Lett. **24**(28), 8453–8464 (2024).
[21]S.-H. Sunwoo, K.-H. Ha, S. Lee, N. Lu, and D.-H. Kim, "Wearable and implantable soft bioelectronics: Device designs and material strategies," Annu. Rev. Chem. Biomol. Eng. **12**, 359–391 (2021).
[22]B. Lee, M. K. Koripalli, Y. Jia, J. Acosta, M. S. E. Sendi, Y. Choi, and M. Ghovanloo, "An implantable peripheral nerve recording and stimulation system for experiments on freely moving animal subjects," Sci. Rep. **8**(1), 6115 (2018).
[23]K. Sim, F. Ershad, Y. Zhang, P. Yang, H. Shim, Z. Rao, Y. Lu, A. Thukral, A. Elgalad, Y. Xi, B. Tian, D. A. Taylor, and C. Yu, "An epicardial bioelectronic patch made from soft rubbery materials and capable of spatiotemporal mapping of electrophysiological activity," Nat. Electron. **3**(12), 775–784 (2020).
[24]G. D. Cha, W. H. Lee, S. H. Sunwoo, D. Kang, T. Kang, K. W. Cho, M. Kim, O. K. Park, D. Jung, J. Lee, S. H. Choi, T. Hyeon, and D. H. Kim, "Multifunctional injectable hydrogel for *in vivo* diagnostic and therapeutic applications," ACS Nano **16**(1), 554–567 (2022).
[25]G. Li and C. F. Guo, "PEDOT:PSS-based intrinsically soft and stretchable bioelectronics," Soft Sci. **2**(2), 7 (2022).
[26]S. Gong, L. W. Yap, Y. Zhu, B. Zhu, Y. Wang, Y. Ling, Y. Zhao, T. An, Y. Lu, and W. Cheng, "A soft resistive acoustic sensor based on suspended standing nanowire membranes with point crack design," Adv. Funct. Mater. **30**(25), 1910717 (2020).
[27]J. Kim, G. D. Cha, M. Kim, S. P. Lee, S. H. Sunwoo, and D. H. Kim, "Soft cardiac patch using a bifacial architecture of adhesive/low-impedance hydrogel nanocomposites and highly conductive elastomer nanocomposites," Adv. NanoBiomed. Res. **5**(3), 2400143 (2024).
[28]Y. Lin, T. Fang, C. Bai, Y. Sun, C. Yang, G. Hu, H. Guo, W. Qiu, W. Huang, L. Wang, Z. Tao, Y. Q. Lu, and D. Kong, "Ultrastretchable electrically self-healing conductors based on silver nanowire/liquid metal microcapsule nanocomposites," Nano Lett. **23**(23), 11174–11183 (2023).
[29]M. Wang, Z. Yan, T. Wang, P. Cai, S. Gao, Y. Zeng, C. Wan, H. Wang, L. Pan, J. Yu, S. Pan, K. He, J. Lu, and X. Chen, "Gesture recognition using a bioinspired learning architecture that integrates visual data with somatosensory data from stretchable sensors," Nat. Electron. **3**(9), 563–570 (2020).
[30]Y. Zhang, H. Zhu, S. An, W. Xing, B. Fu, P. Tao, W. Shang, J. Wu, M. D. Dickey, C. Song, and T. Deng, "Chameleon-inspired tunable multi-layered infrared-modulating system via stretchable liquid metal microdroplets in elastomer film," Nat. Commun. **15**(1), 5395 (2024).
[31]Y. Ling, K. Guo, B. Zhu, B. Prieto-Simon, N. H. Voelcker, and W. Cheng, "High-adhesion vertically aligned gold nanowire stretchable electrodes: Via a thin-layer soft nailing strategy," Nanoscale Horiz. **4**(6), 1380–1387 (2019).
[32]K. W. Cho, S. H. Sunwoo, Y. J. Hong, J. H. Koo, J. H. Kim, S. Baik, T. Hyeon, and D. H. Kim, "Soft bioelectronics based on nanomaterials," Chem. Rev. **122**(5), 5068–5143 (2022).
[33]S. Cheng, Z. Lou, L. Zhang, H. Guo, Z. Wang, C. Guo, K. Fukuda, S. Ma, G. Wang, T. Someya, H. M. Cheng, and X. Xu, "Ultrathin hydrogel films toward breathable skin-integrated electronics," Adv. Mater. **35**(1), e2206793 (2023).
[34]Z. Liu, H. Wang, P. Huang, J. Huang, Y. Zhang, Y. Wang, M. Yu, S. Chen, D. Qi, T. Wang, Y. Jiang, G. Chen, G. Hu, W. Li, J. Yu, Y. Luo, X. J. Loh, B. Liedberg, G. Li, and X. Chen, "Highly stable and stretchable conductive films through thermal-radiation-assisted metal encapsulation," Adv. Mater. **31**(35), e1901360 (2019).
[35]O. Awartani and M. D. Dickey, "Making soft and reconfigurable electronics with liquid metals," Phys. Today **76**(6), 54–55 (2023).
[36]K. Y. Kwon, V. K. Truong, F. Krisnadi, S. Im, J. Ma, N. Mehrabian, T. Kim, and M. D. Dickey, "Surface modification of gallium-based liquid metals: mechanisms and applications in biomedical sensors and soft actuators," Adv. Intell. Syst. **3**(3), 2000159 (2021).
[37]Y. Lin, H. Wang, W. Qiu, C. Ye, and D. Kong, "Liquid metal-based self-healing conductors for flexible and stretchable electronics," ACS Appl. Mater. Interfaces **16**(33), 43083–43092 (2024).
[38]H. Hu, H. Huang, M. Li, X. Gao, L. Yin, R. Qi, R. S. Wu, X. Chen, Y. Ma, K. Shi, C. Li, T. M. Maus, B. Huang, C. Lu, M. Lin, S. Zhou, Z. Lou, Y. Gu, Y. Chen, Y. Lei, X. Wang, R. Wang, W. Yue, X. Yang, Y. Bian, J. Mu, G. Park, S. Xiang, S. Cai, P. W. Corey, J. Wang, and S. Xu, "A wearable cardiac ultrasound imager," Nature **613**(7945), 667–675 (2023).
[39]J. Ma, F. Krisnadi, M. H. Vong, M. Kong, O. M. Awartani, and M. D. Dickey, "Shaping a soft future: Patterning liquid metals," Adv. Mater. **35**(19), 2205196 (2023).
[40]M. D. Dickey, "Stretchable and soft electronics using liquid metals," Adv. Mater. **29**(27), 1606425 (2017).
[41]Q. Zhuang, K. Yao, C. Zhang, X. Song, J. Zhou, Y. Zhang, Q. Huang, Y. Zhou, X. Yu, and Z. Zheng, "Permeable, three-dimensional integrated electronic skins with stretchable hybrid liquid metal solders," Nat. Electron. **7**(7), 598–609 (2024).
[42]S.-Y. Tang, C. Tabor, K. Kalantar-Zadeh, and M. D. Dickey, "Gallium liquid metal: The Devil's elixir," Annu. Rev. Mater. Res. **51**, 381–408 (2025).
[43]S. H. Sunwoo, S. I. Han, D. Jung, M. Kim, S. Nam, H. Lee, S. Choi, H. Kang, Y. S. Cho, D. H. Yeom, M. J. Cha, S. Lee, S. P. Lee, T. Hyeon, and D. H. Kim, "Stretchable low-impedance conductor with Ag-Au-Pt core-shell-shell nanowires and in situ formed Pt nanoparticles for wearable and implantable device," ACS Nano **17**(8), 7550–7561 (2023).
[44]S. H. Kim, H. Seo, J. Kang, J. Hong, D. Seong, H. J. Kim, J. Kim, J. Mun, I. Youn, J. Kim, Y. C. Kim, H. K. Seok, C. Lee, J. B. H. Tok, Z. Bao, and D. Son, "An ultrastretchable and self-healable nanocomposite conductor enabled by autonomously percolative electrical pathways," ACS Nano **13**(6), 6531–6539 (2019).
[45]H. Joo, D. Jung, S. H. Sunwoo, J. H. Koo, and D. H. Kim, "Material design and fabrication strategies for stretchable metallic nanocomposites," Small **16**(11), 1906270 (2020).
[46]S. Nam, C. Park, S. H. Sunwoo, M. Kim, H. Lee, M. Lee, and D. H. Kim, "Soft conductive nanocomposites for recording biosignals on skin," Soft Sci. **3**(3), 28 (2023).
[47]S. H. Sunwoo, S. I. Han, H. Kang, Y. S. Cho, D. Jung, C. Lim, C. Lim, M. jin Cha, S. P. Lee, T. Hyeon, and D. H. Kim, "Stretchable low-impedance nanocomposite comprised of Ag–Au Core–shell nanowires and Pt black for epicardial recording and stimulation," Adv. Mater. Technol **5**(3), 1900768 (2020).
[48]Y. Murakawa, T. Yamashita, Y. Kanese, and M. Omata, "Can a class III antiarrhythmic drug improve electrical defibrillation efficacy during ventricular fibrillation?," J. Am. Coll. Cardiol. **29**(3), 688–692 (1997).
[49]D. S. Khoury, M. D. Assar, and H. Sun, "Pharmacologic enhancement of atrial electrical defibrillation efficacy: Role of ibutilide," J. Interv. Card. Electrophysiol. **1**(4), 291–298 (1997).
[50]A. Sahasrabudhe, L. E. Rupprecht, S. Orguc, T. Khudiyev, T. Tanaka, J. Sands, W. Zhu, A. Tabet, M. Manthey, H. Allen, G. Loke, M. J. Antonini, D. Rosenfeld, J. Park, I. C. Garwood, W. Yan, F. Niroui, Y. Fink, A. Chandrakasan, D. V. Bohórquez, and P. Anikeeva, "Multifunctional microelectronic fibers enable wireless modulation of gut and brain neural circuits," Nat. Biotechnol. **42**(6), 892–904 (2024).
[51]J. S. Marion, N. Gupta, H. Cheung, K. Monir, P. Anikeeva, and Y. Fink, "Thermally drawn highly conductive fibers with controlled elasticity," Adv. Mater. **34**(19), 2201081 (2022).
[52]I. C. Garwood, A. J. Major, M.-J. Antonini, J. Correa, Y. Lee, A. Sahasrabudhe, M. K. Mahnke, E. K. Miller, E. N. Brown, and P. Anikeeva, "Multifunctional fibers enable modulation of cortical and deep brain activity during cognitive behavior in macaques," Sci. Adv. **9**(40), eadh0974 (2023).
[53]A. Canales, X. Jia, U. P. Froriep, R. A. Koppes, C. M. Tringides, J. Selvidge, C. Lu, C. Hou, L. Wei, Y. Fink, and P. Anikeeva, "Multifunctional fibers for simultaneous optical, electrical and chemical interrogation of neural circuits in vivo," Nat. Biotechnol. **33**(3), 277–284 (2015).
[54]S. Nam, G. D. Cha, S. H. Sunwoo, J. H. Jeong, H. Kang, O. K. Park, K. Y. Lee, S. Oh, T. Hyeon, S. H. Choi, S. P. Lee, and D. H. Kim, "Needle-like multifunctional biphasic microfiber for minimally invasive implantable bioelectronics," Adv. Mater. **36**(36), 2404101 (2024).

[55]J. Larson, L. Rich, A. Deshmukh, E. C. Judge, and J. J. Liang, "Pharmacologic Management for ventricular arrhythmias: Overview of anti-arrhythmic drugs," J. Clin. Med. **11**(11), 3233 (2022).
[56]S. Guarini, "A highly reproducible model of arterial thrombosis in rats," J. Pharmacol. Toxicol. Methods **35**(2), 101–105 (1996).
[57]L. Z. Sun, Z. G. Wang, Y. Liu, and G. Wang, "Elastography method for reconstruction of nonlinear breast tissue properties," Int. J. Biomed. Imaging **2009**, 406854.
[58]N. N. A. Nazri, H. Aris, Z. Sauli, and W. M. W. Norhaimi, "Assessment of stress and strain on women's breast tissue caused by single round malignant tumor," AIP Conf. Proc. **2203**, 020016 (2020).
[59]A. Samani, J. Zubovits, and D. Plewes, "Elastic moduli of normal and pathological human breast tissues: An inversion-technique-based investigation of 169 samples," Phys. Med. Biol **52**(6), 1565–1576 (2007).